A EUROPEAN JOURNAL

CHEMPHYSCHEM

OF CHEMICAL PHYSICS AND PHYSICAL CHEMISTRY

Accepted Article

Title: Luminescent Spectral Conversion to Improve the Performance of Dye-sensitized Solar Cells

Authors: Zahra Hosseini, Nima Taghavinia, and Eric Wei-Guang Diau

To be cited as: *ChemPhysChem* 10.1002/cphc.201700920

Link to VoR: http://dx.doi.org/10.1002/cphc.201700920

A Journal of

ChemPubSoc Europe

WILEY-VCH

www.chemphyschem.org

10.1002/cphc.201700920

WILEY-VCH

Luminescent Spectral Conversion to Improve the Performance of Dye-sensitized Solar Cells

Zahra Hosseini,*[a] Nima Taghavinia,[b] and Eric Wei-Guang Diau[c]

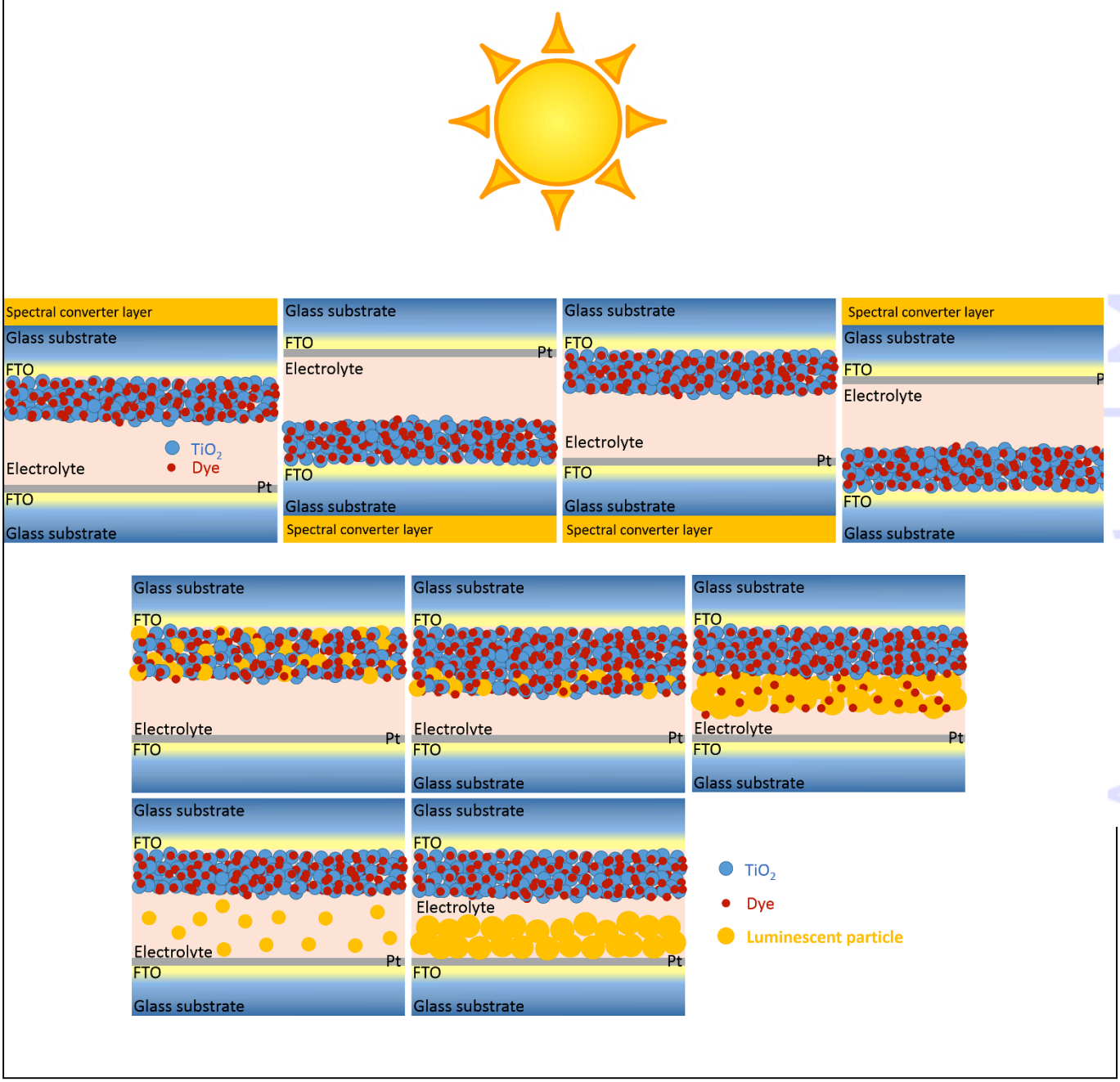

Abstract: Relative to the broad-band solar spectrum, a narrow range of spectral absorption of photovoltaic (PV) devices is considered an important reason for the efficiency of harvesting light of these devices being less than unity. Having the narrowest spectral response to solar radiation among all PV devices, a dye-sensitized solar cell (DSSC) suffers severely from this loss. Luminescent spectral conversion provides a mechanism to manipulate and to adapt the incident solar spectrum through converting solar photons into energies that are more effectively captured by a PV device through photoluminescence. This mechanism is particularly helpful for DSSC because there is a lot of flexibility in both the choice of the light-harvesting materials and the architecture of the DSSC. Here we review and discuss recent advances in the fields of luminescent spectral conversion for DSSCs. The focus is on the architectural design of DSSCs. The complication, advantages and new functionalities offered in each configuration are discussed. The loss mechanisms are investigated and important parameters governing the spectral conversion mechanism of a DSSC are introduced.

1. Introduction

All photovoltaic devices exhibit a limited spectral response relative to the wide-band solar spectrum. The response of a PV device is described by its efficiency of conversion of incident photons to current (IPCE), which is a measure of the efficiency of a device in converting incident light into electrical energy at a given wavelength. Figure 1, which shows the IPCE of various PV devices, makes clear that these devices exhibit a varied performance across the spectrum. Silicon solar cells, having the best performance, exhibit a high IPCE in the visible and near-infrared (NIR) regions. The efficient region of thin-film chalcogenide cells (e.g., copper indium gallium selenide (CIGS) and copper zinc tin sulfide (CZTS)) is narrower, losing photons of both IR and short-wavelength visible light. For organic photovoltaic (OPV) devices, dye-sensitized solar cells (DSSC) and perovskite solar cells (PSC), this spectral window is even narrower. The inefficient performance of these devices in some spectral regions is attributed mainly to the limited absorption of the materials that serve as light absorbers. The spectral absorption is tunable, to some extent, through careful selection of the light-harvesting material, however there are additional loss mechanisms that vary with the intrinsic nature of the solar cell.

[a] Dr. Z. Hosseini
Faculty of Advanced Technologies
Shiraz University, Shiraz 71946-84560 (Iran)
E-mail: zahrahosseini@shirazu.ac.ir
[b] Prof. N. Taghavinia
Physics Department and Institute for Nanoscience and Nanotechnology
Sharif University of Technology, Tehran 14588 (Iran)
[c] Prof. E. W.-G. Diau
Department of Applied Chemistry and Institute of Molecular Science
National Chiao Tung University, Hsinchu 30010 (Taiwan)

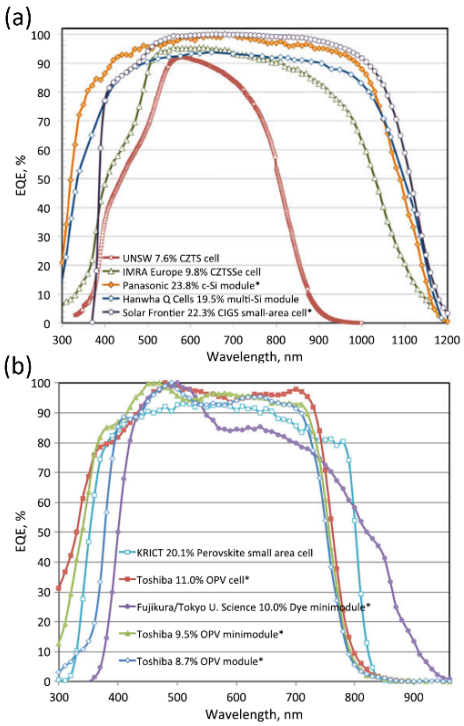

Figure 1. (a) IPCE for silicon and chalcogenide cells and modules reported in tables of solar cell efficiency (version 48) [1]. (b) IPCE for perovskite, dye-sensitized and organic solar cells reported in these tables (Version 45) [2]. Reproduced with permission.

In DSSC, the dye molecules are responsible for the light absorption. Dye molecules of various kinds with varied absorption bands and absorption coefficients have been developed for application in DSSC. The article by Hagfeldt et al. [3] provides a comprehensive review and introduction of dye molecules. The absorption spectra of dye molecules of several kinds appear in Figure 2. The spectral distribution of the photon flux for the standard global (air mass 1.5, AM1.5G) solar spectrum is also plotted in Figure 2 to reveal the available photons that are not absorbed by each dye and that no dye absorbs photons over the entire solar spectrum. A compromise between absorption width and absorption coefficient of a dye impedes a possibility to have a DSSC with intense absorption over a wide range of the solar spectrum. The problems related to the adsorption and stability of some dyes make impossible their facile utilization in DSSC. Ru dyes such as N719 are the most conventional dyes; their band gap is about 1.6 eV [4]. Although they can absorb a wide band in the wavelength range between 300 and 800 nm, still 50 % of solar radiation in the ultraviolet and infrared regions is not utilized in DSSC sensitized with these dye molecules. Their absorption coefficients are also small, typically 5000−20000 M^{-1} cm^{-1} [3]. A typical strategy to compensate for these small coefficients is to increase the thickness of the TiO_2 mesoporous layer so that the quantity of

loaded dye can be correspondingly increased to absorb a significant portion of the incident photons [5]. Though increasing the thickness of the TiO_2 mesoporous layer negatively affects the photogenerated charge collection efficiency. Moreover, this approach is inapplicable for solid-state or flexible DSSC, for which the TiO_2 layer must be thin. In such cases, dye molecules with large absorption coefficients must be used in exchange for the loss of the absorption band width. Porphyrins, phthalocyanines and some organic dyes possess the largest absorption coefficients [3,6].

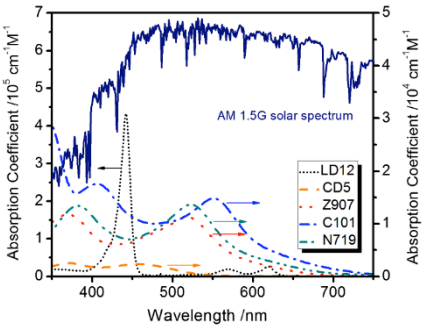

Figure 2. Absorption spectra of dye molecules of several kinds. LD12 is a porphyrin, CD5 is an organic dye and Z907, C101 and N719 are Ru based dyes. The spectral distribution of the photon flux for the standard-air-mass-1.5 global (AM1.5G) solar spectrum is also plotted.

Several strategies to achieve a panchromatic spectral response in DSSC have been applied [7,8]. Co-sensitization with multiple dyes has been tested widely with various dye molecules [9–12]; according to this approach, dye molecules of two or more kinds with complementary absorption bands are adsorbed on the mesoporous TiO_2 layer. As the number of adsorption sites available for each dye is limited, the application of dyes with large absorption coefficients is more favorable for co-sensitization in DSSC. Avoiding unfavorable interactions among the various dye molecules is the main challenge of this approach [7]. A tandem architecture for solar cells is also used to adapt the cell to improve the use of the solar spectrum [7,13]; in a tandem structure, solar cells sensitized with various dye molecules, and thereby varied absorption spectra, are stacked above one another; this approach considerably complicates the fabrication and increases the total cost of manufacturing [7,13]. In another approach, highly luminescent energy-relay dyes (ERD), dissolved inside the electrolyte, absorb energetic photons and transfer their energy to the sensitizing dye via a Forster resonance-energy transfer (FRET) [14–17]. The choice of ERD and sensitizing dye is important in this approach as their absorption bands must be complementary, with effective overlap between the emission band of the ERD and the absorption band of the sensitizing dye [7,14]. An ERD is limited by the requirements that it must be soluble in, but not greatly quenched by, the electrolyte media, as well as having large molar absorption coefficients. This limited efficiency of the FRET restricts the attainable light harvesting.

Luminescent spectral conversion is another approach to extend the light-harvesting ability of a DSSC. According to this approach the parts of the incident radiation from the wavelengths that the cell absorbs poorly are converted to wavelengths at which the cell absorbs better. In this conversion, either high-energy photons are converted to low-energy photons or the reverse; the former is called down-conversion (DC) or down-shifting (DS); the latter is up-conversion (UC). In down-conversion a high-energy photon is converted to two low-energy photons whereas in DS only one low-energy photon is emitted after the absorption of each photon so that a portion of the photon energy is lost through thermal relaxation. The UC is the reverse of DC such that two or more low-energy photons are combined to yield one photon of greater energy. A detailed description of UC, DC and DS is available in [18–28]. Figure 3 presents a simple example of wavelength conversion shifting of non-absorbed parts of the spectrum to a region of greater IPCE. A DSSC sensitized with squaraine (SQ1) exhibits a sharply decreased IPCE for wavelengths less than 550 nm in the visible part of the spectrum. The incorporation of a luminescent material such as CaZnOS:Eu^{2+} that absorbs in the spectral region of wavelength less than 600 nm and emits at 600-700 nm would improve the light-harvesting efficiency by widening the absorption band of the device [29].

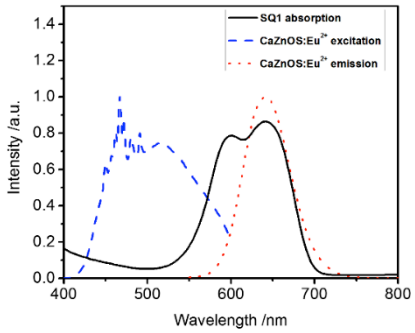

Figure 3. Absorption spectrum of SQ1 adsorbed on TiO_2 film and excitation (λ_{em}/nm=650) and emission (λ_{ex}/nm=466) spectra of CaZnOS:Eu^{2+} phosphor.

In 1979 Hovel et al. first applied the concept of spectral conversion with a luminescent layer (LL) placed above various Si or thin-film PV cells [30]. This approach has since been utilized to diminish the spectral mismatch losses in various PV devices such as Si solar cells [20,31–37], CdS/CdTe solar cells [20,34,38–42], and copper-indium-gallium-selenide (CIGS) solar cells [34,39,43,44]. For this purpose, a luminescent material as a transparent layer is placed above or at the bottom of the solar cell for the DC and UC processes respectively [24,45–47]. An application of this concept to the DSSC appeared in the literature only in 2006. Similarly, to utilize the UV photons, Liu et al. placed a transparent LL of uniform $LaVO_4$:Dy nanocrystals on the front

surface of DSSC sensitized with N3 dye [48]. The spectral-conversion mechanism was also utilized to improve the light harvesting and the stability of perovskite solar cells [49–51].

As the light-absorbing material is fixed in the Si, CdS/CdTe or CIGS solar cells, the available spectral region for the DC or UC is settled and the choice of luminescent material as spectral converter is limited accordingly, but in the DSSC the available spectral region for the conversion and thereby the choice of the luminescent material is readily variable on changing the sensitizing dye [29]. Use of a luminescent material inside Si or thin-film solar cells is impractical because of their rigid structure, but a flexible structural design of the DSSC provides a possibility to apply a luminescent material in the various structures, inside or outside the DSSC [29,52–55].

In this review we focus on the structural design of DSSC to apply luminescent spectral converters. We first discuss the requirements of a luminescent material as a spectral converter and introduce the best luminescent candidates for this application. This description is short because several comprehensive discussions of key requirements and properties of the spectral- conversion mechanism exist [18–28,56]. We then review various possible architectures for a DSSC with a spectral converter included, discussing the challenges, advantages and disadvantages of each configuration. We further summarize the efforts made so far and what further can be tried, to achieve a performance of a DSSC significantly enhanced from the spectral conversion of the solar radiation.

Zahra Hosseini received her B.Sc. and M.Sc. degrees in physics from Shiraz University and Sharif University of Technology (SUT) in Iran, in 2005 and 2008, respectively. She obtained her Ph.D. in nanotechnology under the supervision of Prof. Nima Taghavinia, from Institute for Nanoscience and Nanotechnology, Sharif University of Technology in 2014. Since 2015 she has been a faculty member of Faculty of Advanced Technologies at Shiraz University. Her research interests include optoelectronic devices, nanostructured solar cells, and photocatalysis.

Nima Taghavinia received his B.Sc. and M.Sc. degrees in physics at Sharif University of Technology, Iran, in 1994 and 1996, respectively. He received a Ph.D. in Materials Science from Tohoku University, Japan, in 2002. Since then he has been a faculty member of the Physics Department and a member of Institute for Nanoscience and Nanotechnology at Sharif University of Technology. His group conducts research on printable solar cells.

Eric Wei-Guang Diau started his research in 2001 in Department of Applied Chemistry and Science of Molecular Science, National Chiao Tung University (NCTU), Taiwan. He is interested on studying relaxation kinetics, in particular interfacial electron transfer and energy transfer dynamics in many solar energy conversion systems. His current research is focusing on the developments of novel functional materials for next-generation solar cells, including perovskite solar cells. He received “Outstanding Research Award” from MRS Spring Meeting & Exhibit on April, 2014 and “Sun Yat Sen Academic Award” from Sun Yat Sen Academic and Cultural Foundation on October, 2014. He has published over 175 peer-reviewed papers with H-index 51. He has been granted over 14 patents. He is currently Distinguished Professor at NCTU.

2. Luminescent Materials for Spectral Conversion

A luminescent material can broaden the light-harvesting band of a DSSC by converting the incident spectrum in a way that photons with wavelengths outside an absorption range of dye molecules become converted to photons with wavelengths within the absorption band of the sensitizing dye. For this purpose, a luminescent material must satisfy specific requirements to maximize the benefits from the application of this strategy as follows. The appropriate luminescent material possesses a luminescence spectrum that matches the absorption spectrum of the active layer in the solar cell. The excitation band of the luminescent material covers well the wavelength region in which the IPCE of the solar cell is small. To avoid loss due to re-absorption of photons emitted by a luminescent species, the overlap between the emission spectrum and the excitation spectrum of the luminescent material should become minimized. The luminescent material should also possess a large quantum efficiency (QE) for luminescence, large absorption coefficient, adequate photochemical stability and modest cost for practical applications.

Suitable candidates for a luminescent material in the spectral-conversion strategy are inorganic quantum dots (QD) or organic dyes or inorganic phosphors. QDs exhibit wide absorption bands large emission intensity and adequate photochemical stability, but reabsorption loss is a serious problem in their use due to a large overlap between their absorption and emission bands [46,57,58]. Organic dyes exhibit large absorption coefficients and a large QE, but they typically have a narrow absorption band that considerably overlaps their emission band; that is, the absorption loss is a problem for an organic dye, and the photochemical stability of organic dyes is generally poor [46,57,58].

Inorganic phosphors have almost all characteristics required for an application in a spectral-conversion strategy – satisfactory QE, excellent photochemical stability and modest cost. They exhibit wide absorption bands with typically little or no overlap

between their absorption and emission bands, but they have small absorption coefficients, for which compensation through increasing the concentration of the material or the thickness of the LL is practicable [18,20,21,24,25,46,58]. As spectral converters, inorganic phosphors are used more than luminescent materials of other classes.

As mentioned above, because of the flexibility of the sensitizing dye in a DSSC and the diverse luminescent materials, a wide selection of luminescent material or dye couples exists for application in the spectral-conversion strategy. To facilitate a choice, the requirements of a luminescent material have been quantified through defining some magnitudes suggested by Alonso-Álvarez et al. [41], summarized as follows.

1. *Radiative overlap* (RO). If absorption and emission bands of a luminescent material are not separate, the emitted photons might be absorbed by the luminescent material before reaching the dye molecules. Re-absorption can be a loss channel as re-absorbed photons might not be re-emitted by a luminescent material unless the luminescent QE is 100 %. The chance of losing a photon through re-absorption is proportional to the fraction of the emission spectrum that overlaps the absorption one, defined as RO [41]:

$$RO = \frac{\int Abs(\lambda)Em(\lambda)d\lambda}{\int Em(\lambda)d\lambda} \quad (1)$$

in which *Abs*(λ) and *Em*(λ) represent the absorption and emission of the luminescent material, respectively.

2. *Absorption spectral matching* (ASM). The luminescent material should have a broad absorption that matches the region of the solar spectrum not absorbed by the sensitizing dye in the DSSC. In a DSSC with a large efficiency of injection and collection, this region matches well with the wavelength region of small IPCE. The ASM quantity is thus calculated as [41]

$$ASM = \frac{\int Abs(\lambda)AM1.5G(\lambda)(1-IPCE(\lambda))d\lambda}{\int AM1.5G(\lambda)(1-IPCE(\lambda))d\lambda} \quad (2)$$

in which *AM*1.5G(λ) is the incident solar spectrum and *IPCE*(λ) is the efficiency of conversion of incident photons to a current of the device.

3. *Parasitic absorption* (PA). If the absorption band of the luminescent material overlaps the spectral band in which the bare DSSC exhibits a large IPCE, the luminescent material absorbs photons efficiently used by the solar cell. As the luminescent material does not necessarily emit after the absorption of these photons, the overlap between the absorption band of a luminescent material and the IPCE spectrum of a DSSC provides a loss mechanism, quantified as [41]

$$PA = \frac{\int Abs(\lambda)AM1.5G(\lambda)IPCE(\lambda)d\lambda}{\int AM1.5G(\lambda)IPCE(\lambda)d\lambda} \quad (3)$$

4. *Emission spectral matching* (ESM). So that the converted photons participate in the current generation, the emission spectrum of the luminescent material must effectively overlap the absorption band of the dye molecules; these wavelengths then provide a large IPCE of a device. The ESM is thus defined as the fraction of the emission that overlaps the IPCE [41]:

$$ESM = \frac{\int Em(\lambda)IPCE(\lambda)d\lambda}{\int Em(\lambda)d\lambda} \quad (4)$$

An ideal luminescent material to be used in the spectral conversion strategy not only has QE=1 and RO=0, but also must match the sensitizing dye in the DSSC such that ASM, ESM=1 and PA=0.

The absorption coefficient of a luminescent material is another factor that governs the enhancement achievable with this strategy; it plays a crucial role especially in an architecture in which the applicable concentration of luminescent material is limited. Further discussion follows including the limitations of various architectures.

For clarity of the impact of these factors on the performance of a spectral converter, the factors defined for three luminescent materials that serve as spectral converters of a SQ1- sensitized DSSC are summarized in Figure 4. We reported the results of the application of these materials in an identical architecture on a SQ1-sensitized DSSC [29]. The large ASM and ESM, with the small RO and PA, confirm the effective match of these three luminescent materials with the SQ1 dye for an application in a spectral-conversion strategy, as proved by the considerably enhanced light harvesting and thereby efficiency of the solar cell The best improvement, about 54 %, achieved with $CaAlSiN_3:Eu^{2+}$ as spectral converter, indicates that the QE must here be the critical factor that governs the performance of the spectral converters [29].

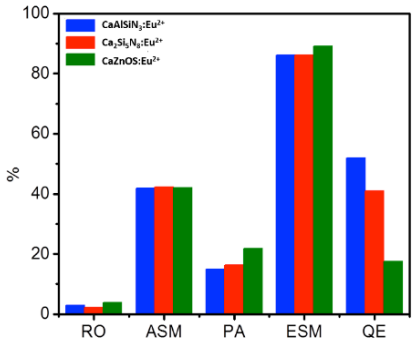

Figure 4. Quantified figures of merit of the three phosphors -- $CaAlSiN_3:Eu^{2+}$, $Ca_2Si_5N_8:Eu^{2+}$ and $CaZnOS:Eu^{2+}$ -- as spectral converters for a SQ1-sensitized DSSC.

In the following sections, we describe a possible structural design of a DSSC with a spectral converter in two categories -- structures with the spectral converter outside or inside the DSSC.

3. Application of the spectral converter outside the DSSC

To apply the strategy of spectral conversion, a layer containing the appropriate luminescent material might be placed outside the DSSC on the working-electrode (WE) side or on the counter-electrode (CE) side; the choice of that position of the luminescent layer (LL) outside the DSSC is based mainly on the transparency of this layer. Figure 5 shows a scheme of four possible configurations for application of a spectral converter outside the DSSC. In configurations a & b, the LL is placed on the WE, whereas in configurations c & d on the CE. These four structures can be classified as transmissive or reflective configurations. In a transmissive structure, the incident photons pass through the LL before reaching the solar cell, i.e. configurations a & d, whereas in the reflective structures the incident light irradiates the solar cell first, i.e. configurations b & c.

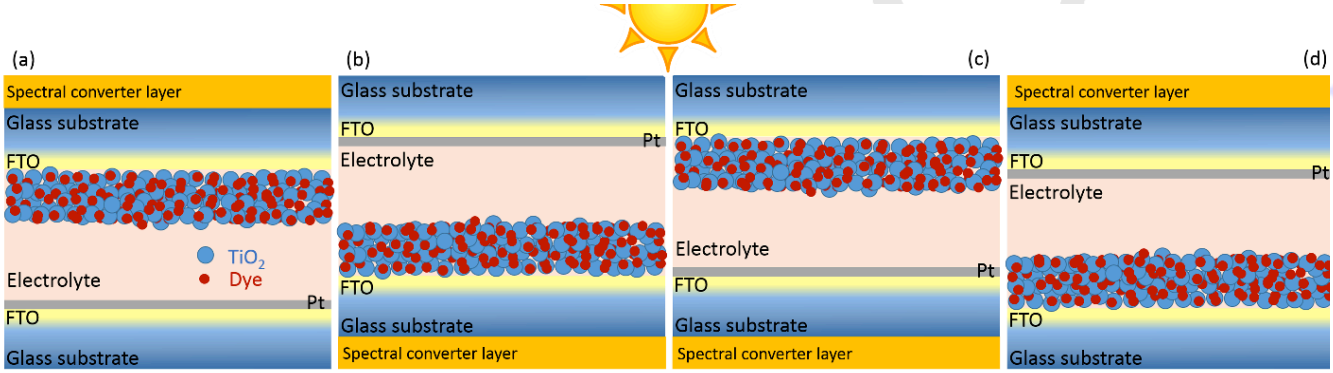

Figure 5. Schemes of four configurations to apply a spectral converter outside a DSSC. (a) transmissive structure with LL on the WE side, (b,c) reflective structures with LL on the WE and CE sides respectively, (d) transmissive structure with LL on the CE side.

Configuration a (Figure 5a) is a transmissive structure in which the luminescent layer is placed on the WE side; the device is illuminated from the same side, i.e. front illumination. As incident photons pass through the LL before entering the DSSC, the PA can cause an appreciable loss that weakens the performance of the cell [59–62]. A careful choice of luminescent material or dye couple with zero or negligible PA is thus necessary for a fabrication of configuration a. Moreover, the LL should be transparent in this configuration. Scattering effect in LL cause a loss channel by supressing incident photons from reaching the luminescent particles or dye molecules. More discussion on this effect is provided in the following.

The structure in which a LL is placed on the WE side with front illumination is commonly used for the purpose of conversion of UV light to visible photons. A secondary benefit is thus gained through the spectral conversion because the LL serves as both UV cut layer and light-conversion layer [48,59–63]. Not only does the light-harvesting efficiency improve but also the DSSC lifetime increases as a result of suppressing UV photons from reaching the dye molecules. On illuminating the DSSC with the LL on top, the UV part of the solar spectrum becomes absorbed inside the LL. The luminescent particles then emit visible photons that enter the cell and are absorbed by dye molecules with visible photons present in the incident solar spectrum. Liu et al. placed a transparent LL of uniform $LaVO_4$:Dy nanocrystals on a DSSC sensitized with N3 dye [48]; the $LaVO_4$:Dy nanocrystals absorbed UV light and down-converted it to visible light. Compared with an uncoated DSSC, the introduction of the LL on the solar cell greatly enhanced the lifetime of the solar cell, but no enhanced efficiency of power conversion was achieved because of the considerable PA.

With an appropriately chosen luminescent material or dye couple that shows a small PA and large QE, Bella and Griffini achieved enhancements 62 % and 70 % in the efficiency of power conversion of DSSC sensitized with D131 and D205 dye molecules, respectively [61,62]; Lumogen F violet 570 and europium tetrakis dibenzoylmethide triethylammonium (EuD_4TEA) served as spectral converters matched with D131 and D205 dye molecules, respectively. Figure 6 shows normalized absorption and emission spectra of these luminescent materials with the absorption spectrum of the DSSC active layer for two luminescent materials or dye couples [61,62]. These spectra show large ASM and ESM and small RO and PA for both LL. This suitable choice of the luminescent material or dye couple also enhanced the lifetime of the DSSC under long-term (>2000 h) weathering tests in real outdoor conditions.

Other reports on the application of a transparent LL on the WE side of the DSSC are summarized in **Error! Reference source not found.**. Various luminescent materials matched with the sensitizing dyes inside the DSSC have led to a variation among the reported results. The common challenge in all these reports has been a compromise between the opacity of the LL and the

enhanced short-circuit current density (J_{SC}) [48,59–62]. Although a greater concentration of the luminescent species in the LL can absorb and then emit more photons, the enhanced loss due to the PA results in a decreased J_{SC} in the DSSC. Other loss channels such as the RO and fluorescence quenching due to molecular aggregates can also cause a decreased J_{SC} when a luminescent material is used at a large concentration in the LL [61]. A large absorption coefficient and a large luminescent quantum efficiency are parameters that compensate the loss caused by the PA or RO through providing the possibility of a smaller concentration of luminescent material. Employing the plasmonic effect of metallic nanoparticles also improves the performance of a spectral conversion layer [64–67]. Ahmed et al. applied a luminescent down-shifting layer containing core–shell CdSe/ZnS QD on the DSSC in a transmissive configuration [64,68]; not only did the IPCE at small wavelengths not improve compared to the bare device but also this value decreased at larger wavelengths corresponding to the maximum IPCE; these phenomena are attributed to the small QE and non-zero PA respectively. To circumvent this problem, Ahmed et al. used Ag nanoparticles in a luminescent down-shifting layer; the presence of these Ag nanoparticles produced a surface-plasmon response that significantly improved the absorption and emission of the QD. On embedding Ag nanoparticles (15 ppm) in the LL, an emission intensity of the QD increased 60 % was achieved (Figure 7**Error! Reference source not found.**). A significantly enhanced IPCE in the range 300-500 nm (agreeing with the absorption band of the luminescent QD) was consequently attained from the plasmonic LL relative to both the QD LL and the bare DSSC; J_{SC} increased to 12 % in the region 300-800 nm [64].

Although the application of the LL according to configuration a (Figure 5a) might not yield a greatly enhanced efficiency of DSSC power conversion, this configuration eliminates the need for a UV cut-off filter on the DSSC [48,59,61,62,69]. Figure 5b shows a reflective configuration in which the LL is placed on the WE side but the cell is illuminated from the opposite side, i.e. back illumination. This configuration is preferable when the LL is not transparent or an increased concentration of the luminescent material must be used inside the LL; back illumination is thus inevitable. Although in this configuration photons pass through the DSSC before exciting the LL, a fraction of the incident photons is lost before reaching the dye molecules, mainly due to absorption by the electrolyte and the counter electrode [29,53], but this configuration provides advantages such as eliminating a need for an application of a scattering layer inside the DSSC. A LL with a large refractive index or a mirror-like layer at the back of the LL can reflect both transmitted light and emitted photons back to the DSSC [29]; the PA causes no loss in this configuration.

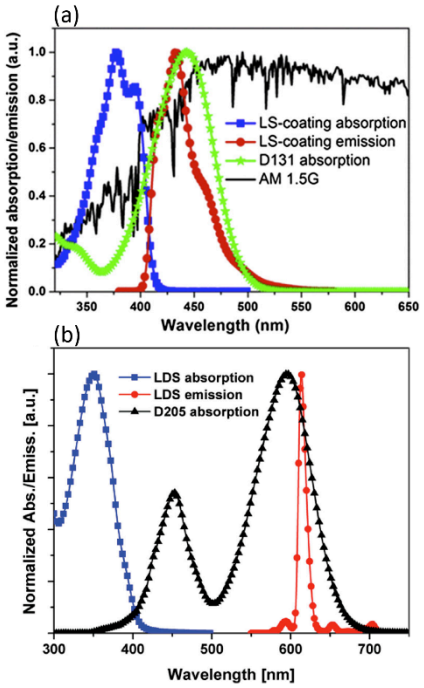

Figure 6. Normalized absorption and emission spectra of LL applied on the DSSC sensitized with D131 (a) [61] and D205 (b) [62] dye molecules, with the absorption spectrum of the related dyes. Reproduced with permission.

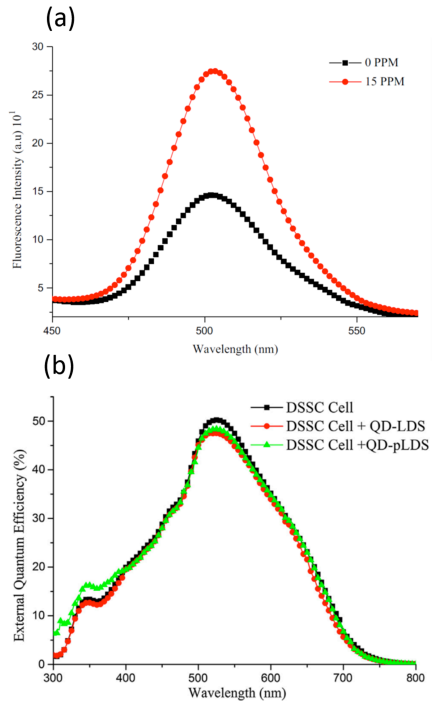

Figure 7. (a) Emission spectra of LL without and with plasmonic particles (15 PPM). (b) IPCE of a DSSC solar cell with no LL, with LL and with a plasmonic LL (pLDS). Reproduced with permission from [64]

Using phosphors doped with Eu^{2+}, we applied a LL on a DSSC sensitized with a near-infrared squaraine dye (SQ1) according to configuration b [29]. The LL shifted the visible part of the solar spectrum to red and near-IR photons well matched with the absorption band of the SQ1 dye. The LL of $CaAlSiN_3:Eu^{2+}$ with quantum efficiency 0.51 of luminescence caused enhanced IPCE about 230 % near 500 nm. Enhancement 54 % s of J_{SC} and efficiency of power conversion was consequently attained. Further investigation showed that the LL caused the enhancement by both down-shifting and back-scattering effects; the former was dominant [29].

To avoid back illumination, an opaque LL can be placed on the CE side of the cell, with the DSSC illuminated from the WE side. This configuration, also reflective, is shown in Figure 5c. In such a configuration, like the configuration in Figure 5b, the opacity of the LL and the PA are not critical issues; the LL can be a thick layer of luminescent material. Another common feature of these two configurations is that the LL can serve as a dual functional layer with both light conversion and light back -scattering functions. There is hence no need to use a scattering layer inside the DSSC, which simplifies the fabrication. The only superiority of configuration c over b is that, on avoiding back illumination, the number of primary incident photons on dye molecules remains constant at all wavelengths after application of the LL; increased overall efficiencies are hence attained in configuration c relative to configuration b. Light absorption by the electrolyte and the counter electrode provides loss mechanisms in configuration c, if the absorption or emission bands of the LL overlap the absorption spectra of these parts of the DSSC. Using the same luminescent material or dye couple ($CaAlSiN_3:Eu^{2+}$/SQ1), we compared these two reflective configurations (b & c) [29]; for configuration c, enhancements 200 % and 40 % were achieved for IPCE (at 500 nm) and J_{SC} respectively. As mentioned above, these values attained 230 % and 54 % for configuration b, but a larger ΔJ_{SC} of the WE-coated device (configuration b) failed to improve the device performances relative to its CE-coated counterpart because the initial loss of incident photons became significant under back-illumination for the WE-coated device. A greater efficiency was thus achieved using configuration c [29].

Further results of the application of the strategy of spectral conversion with fabrication of configuration c are summarized in table 1. Shan et al. put converter β-$NaYF_4:Er^{3+}/Yb^{3+}$ hexagonal nanoplatelets in configuration c as a dual functional layer [70]; approximately 10 % enhanced photocurrent and overall DSSC efficiency were demonstrated on an addition of an external layer on the CE side, but the authors stated that the observed enhancements were due predominantly to the light-reflecting action of the β-$NaYF_4$ nanoplatelet-based layer. The limited UC contribution of the LL, estimated to be ~1 % in terms of both photocurrent and conversion efficiency, was attributed to the small UC efficiency. As UC is a non-linear process that becomes efficient only at a large incident power [24], an application of UC phosphors in the LL is scarcely effective [70,71].

Ramasamy and Kim sought to increase the UC luminescence of a spectral converter in the same configuration by utilizing a plasmonic effect [66]; they placed a layer comprising β-$NaGdF_4$:Yb,Er,Fe nanoparticles (20 nm) and silver particles (1 μm) at the back of the DSSC according to Figure 8a. The UC photoluminescence of the UC nanoparticles was tripled through the surface-plasmon-coupled emission and the large scattering efficiency of the silver particles. The DSSC employing this structure achieved an efficiency 7.04 %, which is about 21.3 % greater than that of the device without a back reflector. The improved performance was attributed to not only the spectral conversion of the NIR to visible light but also the efficient light-reflecting properties of the reflective LL [66]. This effect can be clearly understood from the IPCE spectra shown in Figure 8b for the DSSC with and without the LL.

Figure 5d shows the ultimate configuration in which the LL is placed outside the DSSC; in this transmissive configuration, the LL is placed on the CE side and back illumination is used. The LL must be transparent in both this configuration and configuration a, but it offers no advantage over configuration a. For this reason configuration a is invariably the choice for the application of a transparent LL on the DSSC; there is no report of an application of configuration d.

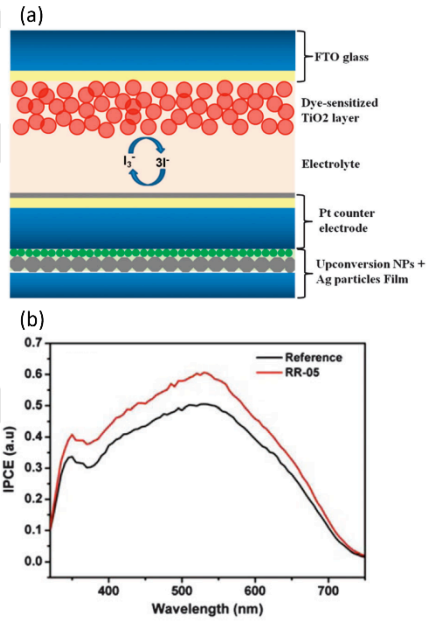

Figure 8. (a) Schematic diagram of a DSSC with UC and plasmonic LL in a reflective configuration. (b) IPCE spectra of DSSC with and without the LL. Reproduced with permission from [66].

A detailed comparison between the performance of a spectral converter layer in reflective and transmissive configurations with an investigation of the related optical loss channels is provided in [53]. The non-unity QE and light absorption by the electrolyte were shown to be the most significant loss channels in the reflective configuration whereas the reflection loss at the interface between air and LL and the escape cone loss played important roles governing the function of the LL in the transmissive configuration. Applying an anti-reflection coating at

the air-glass interface, using Co electrolyte, optimizing the QE of the phosphor and matching the refractive index in the LL were proposed as major modifications to improve the performance. The simulation results presented in [53] indicate that, in the case of use of an ideal luminescent material, the device with a reflective configuration offers a performance superior to that with a transmissive configuration, as the maximum current density calculated by Snaith [72] is attainable by the reflective configuration with an appropriate choice of dye and spectral-converter couple.

Table 1. Figures of merit for DSSCs with the spectral converter outside the cell.

Dye	Luminescent material	Spectral conversion	Cell configuration according to Figure 5	ΔJ_{SC} [%][a]	$\Delta\eta$ [%][a]	Extra function	Reference
N3	$LaVO_4:Dy^{3+}$	DC UV to Vis	a	-18	-5	UV cut	[48]
N719	$YVO_4:Eu^{3+}$	DC UV to Vis	a	4	5	UV cut	[59]
N719	pyrene	DC UV to Vis	a	10	13	-	[60]
D131	Lumogen F Violet 570	DS UV to Vis	a	135	62	UV cut	[61]
D205	EuD_4TEA	DS UV to Vis	a	37	68	UV cut	[62]
N719	$GdVO_4:Dy^{3+}$	DC UV to Vis	a	8	10	-	[63]
-	CdSe/ZnS	DS UV to Vis	a	3	5	-	[64]
N719	1,8-naphthalimide derivatives	DC UV to Vis	a	28	30	UV cut	[69]
-	Yb_2O_3 β-phase $NaYF_4:Yb^{3+},Er^{3+}$	UC NIR to Vis	a	-38 86[b]	-	-	[73]
N719	$NaGdF_4:Eu^{3+}$	DC UV to Vis	a	4	5	Light scatterer	[74]
SQ1	$CaAlSiN_3:Eu^{2+}$	DS Vis to NIR	b c	40 (b) 54 (c)	39 (b) 46 (c)	Back reflecting layer	[29]
N719	β-$NaYF_4:Er^{3+}/Yb^{3+}$	UC NIR to Vis	c	11	9	Back reflecting layer	[70]
N719	YAG:3.0Yb/0.5Er	UC NIR to Vis	c	-	-	Back reflecting layer	[71]
N719	β-$NaGdF_4$:Yb, Er, Fe	UC NIR to Vis	c	25	21	Back reflecting layer	[66]
C106	β-$NaYF_4:Yb^{3+},Er^{3+}$	UC IR to Vis	c	20	19	Back reflecting layer	[54]

[a] The numbers reported for ΔJ_{SC} and $\Delta\eta$ are rounded. [b] under exposure of laser radiation at 980 nm

4. Application of the spectral converter inside the DSSC

Configurations in another class to apply the spectral-conversion strategy in DSSC are those in which the luminescent material is placed inside the DSSC. Diverse configurations depend on the location and method of introduction of the luminescent material. Figure 9 shows the most common configurations to apply the luminescent material inside the DSSC. The luminescent spectral converter might be introduced into the photoanode (Figure 9a and b) or the electrolyte (Figure 9d), or placed on the photoanode (Figure 9c) or counter electrode (Figure 9e) as a separate layer. Although these configurations add some complication to the fabrication of a DSSC, the vicinity of the luminescent material to the sensitizing dye might improve energy transfer between them on eliminating some loss channels. The results reported on applying the spectral converter inside the DSSC are provided in Table 2. The diversity of the results is due not only to the variety of configurations but also to factors such as a variation of the luminescent material or dye couple, and to the varied approaches to make the photoanode layer and the varied concentration of the luminescent material introduced inside the DSSC, but the impact of each factor varies with the configuration. Further discussion of the details of each configuration and the main considerations of each follows.

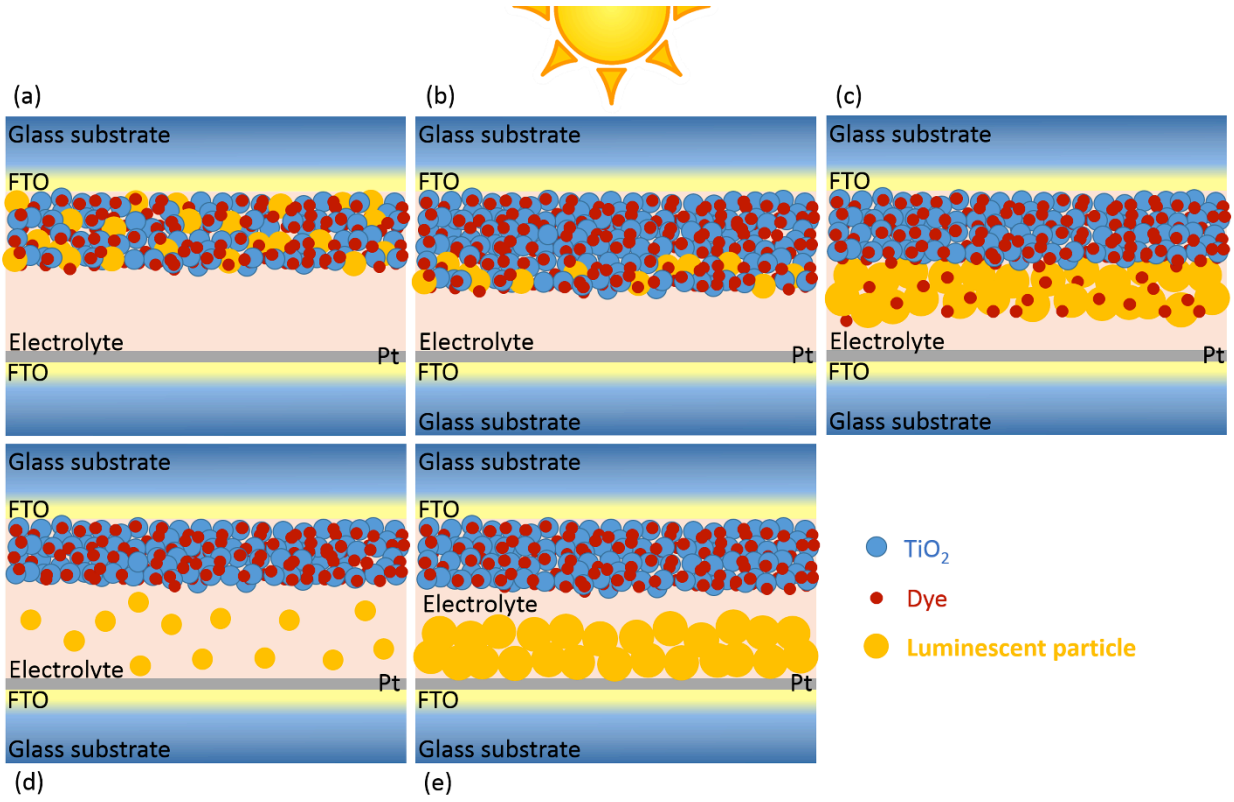

Figure 9. Scheme of DSSC configurations with the spectral converter inside the cell

Table 2. Figures of merit for DSSCs with the spectral converter inside the cell

Dye	Luminescent material	Spectral Conversion	Cell configuration according to Figure 9	ΔJ_{SC} [%][a]	Δη [%][a]	Extra function	Reference
N719	$ZnO:Er^{3+},Tb^{3+}$	UC & DC IR/UV to Vis	a	59	70	*p*-type doping	[75]
N749 N719	$NaYF_4:Yb^{3+},Er^{3+}@NaYF_4$	UC IR to Vis	a	12 6	12 6	*p*-type doping	[76]
N719	$NaYF_4:Yb^{3+},Er^{3+}/TiO_2$	UC IR to Vis	a	8	23	-	[77]
N719	$NaYF_4:Yb^{3+}/Er^{3+}$	UC/DC IR/UV to Vis	a	14	10	-	[78]
N719	$ZnO:Eu^{3+},Dy^{3+}$	DC UV to Vis	a	91	105	-	[79]
N719	$TiO_2:Sm^{3+}$	DC UV to Vis	a	5	9	-	[80]
N719	Lanthanide(sm^{3+},Eu^{3+}) doped TiO_2	DC UV to Vis	a	31	37	-	[81]
N719	Sm_2O_3 modified TiO_2	DC UV to Vis	a	54	73	*p*-type doping	[82]
N719	$SrTiO_3:Sm@SiO_2$	DC UV to Vis	a	27	36	-	[83]
N719	$Gd_2O_3:Er^{3+}/Yb^{3+}$ $Y_3Al_5O_{12}:Ce^{3+}$	UC/DC IR/UV to Vis	a	33	21	-	[84]

N719	$NaYF_4:Er^{3+}/Yb^{3+}$–graphene composites	UC IR to Vis	a	3	4	-	[85]
N719	Er doped TiO_2	UC IR to Vis	a	68	63	-	[86]
N719	$NaxGdF_yO_z:Yb/Er@TiO_2$	UC IR to Vis	a	8	11	Light scaterrer	[87]
N719	TiO_2-Y_2O_3/$Y_2O_2S:Eu^{3+}$	DC UV to Vis	a	16	14	Light scaterrer	[88]
N719	fluorescein	DC UV to Vis	a	5	11	-	[89]
N719	$GdVO_4:Dy^{3+}$	DC UV to Vis	a	-7	3	-	[63]
N719	$YVO_4:Eu^{3+},Bi^{3+}@SiO_2$	DC UV to Vis	a	61	64	Light scaterrer	[90]
N719	$YOF:(Yb^{3+},Er^{3+})$	UC IR to Vis	b	7	24	*p*-type doping	[91]
N719	$Y_2O_3:Dy^{3+}$	DC UV to Vis	b	13	23	- *p*-type doping - UV cut - light scaterrer	[92]
N719	$Ca_3La_{3(1-x)}Eu_{3x}(BO_3)_5$	DC UV to Vis	b	12	35	*p*-type doping	[93]
N719	$Lu_2O_3:(Tm^{3+},Yb^{3+})$	UC IR to Vis	b	9	11	*p*-type doping	[94]
N719	$Y_{0.78}Yb_{0.20}Er_{0.02}F_3$	UC IR to Vis	b	17	35	*p*-type doping	[95]
N719	$Gd_2O_3:Eu^{3+}$	DC UV to Vis	b	12	17	*p*-type doping	[96]
N719	Er^{3+}/Yb^{3+} co-doped LaF_3-TiO_2	UC IR to Vis	b	2	-1	-	[97]
N719	$Gd_2O_3:Sm^{3+}$	DS UV to Vis	b	5	13	*p*-type doping	[98]
N719	$YF_3:Eu^{3+}$	DC UV to Vis	b	12	32	*p*-type doping	[99]
N719	$Y_2O_3:Eu^{3+}$	DC UV to Vis	b	1.4	12	*p*-type doping	[100]
N719	*β*-$NaYF_4:Er^{3+},Yb^{3+}@SiO_2@TiO_2$ HSMs	UC IR to Vis	b	14	11	-	[101]
N719	$CeO_2:Eu^{3+}$	DC UV to Vis	b	17	14	Light scaterrer	[102]
N719	Y_2O_3:Er/Au@TiO_2	UC IR to Vis	b	32	28	Light scaterrer	[67]
N719	*β*-$NaYF_4:Yb^{3+},Er^{3+}@SiO_2$@Au	UC IR to Vis	b	16	15	Light scaterrer	[103]
N719 CSD-01	Yb_2O_3	DC UV to Vis	b	2 17	11 21	Light scaterrer	[104]
N719	$TiO_2:Eu^{3+}$	DC UV to Vis	b	30	38	Light scaterrer	[105]
C106	*t*-$LaVO_4:Dy^{3+}$	DS UV to Vis	b c	4 6	4 3	-	[55]
C106	*β*-$NaYF_4:Yb^{3+},Er^{3+}$	UC IR to Vis	b c	-5 8	-2 5	-	[54]
SQ1	$CaAlSiN_3:Eu^{2+}$	DS	c	64	49	Light scaterrer	[52]

N719	β-$NaYF_4$:Yb^{3+},Er^{3+}/SiO_2/TiO_2	Vis to NIR UC NIR to Vis	c	23	30	Light scaterrer	[106]
N719	$SrAl_2O_4$:Eu^{2+}, Dy^{3+}	DS UV to Vis	c	12	36	Light scaterrer	[107]
-	$Y_3Al_5O_{12}$:Ce	DC UV to Vis	c	15	14	Light scaterrer	[108]
N719	CeO_2:Er,Yb	UC NIR to Vis	c	11	15	Light scaterrer	[109]
N719	perylene	DS Vis to Vis	d	4	16	-	[110]

[a] The numbers reported for ΔJ_{SC} and $\Delta\eta$ are rounded.

In the most common configurations of this type, shown in Figure 9a and b, the luminescent material is introduced into the semiconductor mesoporous layer [63,75–86,90–100,111]. Two approaches were employed to fabricate such structures, of which one is to make the screen printing or doctor-blading paste on mixing the pre-prepared luminescent material powder and the TiO_2-nanoparticle powder [63,75–79,84,85,90–101]. The paste, prepared according to a common procedure used to prepare TiO_2 paste for DSSC [112], then serves to make a composite layer of luminescent material and TiO_2. Another approach is to dope TiO_2 nanoparticles with rare-earth ions [80–83,86,105]. Either the DSSC photoanodes comprise a single composite or doped TiO_2 layer (Figure 9a)[63,76,78,81,82,84,86,90,101] or a transparent TiO_2 layer is positioned between FTO and the composite or doped TiO_2 film (Figure 9b) [91–99,105,111]. When the DSSC is illuminated, the incident photons are absorbed by both dye molecules and luminescent species present in the photoanode layer. The photons absorbed by the dye molecules cause an excitation of electrons to the LUMO level in the dye molecules that are successively injected into the TiO_2 and delivered to the external circuit. In contrast the photons absorbed by the luminescent material are converted to photons that are absorbed by dye molecules and also participate in the current generation. The conversion can be towards photons of greater or lesser energy in an UC or DC/DS process respectively. As mentioned above, the absorption band of a luminescent material covers a spectral band in which the DSSC has little or no absorption. The short-circuit current density hence increases on introducing a luminescent material into the photoanode layer unless new loss channels are introduced on incorporation of the luminescent species inside the DSSC.

In most reports of such configurations, an extra benefit is observed because of the *p*-type doping of TiO_2. Doping TiO_2 with rare-earth ions improves the open-circuit voltage by raising the conduction band and thereby the Fermi level in the TiO_2 because of the *p*-type doping [75,76,86]. This effect is observed even in the case of a paste of mixed TiO_2 nanoparticles and rare-earth-doped luminescent materials to deposit the photoanode layer [91–96,98,99]. After coating, the composite layers are sintered at 450-500 ºC, which is hot enough for diffusion of the rare-earth ions. A small proportion of rare-earth ions, present in the luminescent material, might thus diffuse inside the TiO_2 crystal network and elevate the Fermi level as *p*-type doping [91–96,98,99]. A composite layer of TiO_2 and rare-earth-doped luminescent species might thus also offer a dual functionality and improve both the current density and the open-circuit voltage of the device through light conversion and *p*-type doping respectively.

Such behaviour is reported by most researchers who used rare-earth-ion-doped phosphors as a luminescent material. For example, Wang et al. chose a double-layer structure for the photoanode of a DSSC sensitized with N719 dye consisting of a layer (12 µm) of TiO_2 and a layer (4 µm) of TiO_2 plus yttrium oxyfluoride doped with Yb^{3+} and Er^{3+} [YOF:(Yb^{3+}, Er^{3+})][91]. Through the effect of UC of the near-infrared to visible photons, YOF:(Yb^{3+}, Er^{3+}) increased the photocurrent of the DSSC, and, as a *p*-type dopant, YOF:(Yb^{3+}, Er^{3+}) raised the Fermi level of the TiO_2 film and increased the open-circuit voltage of the DSSC When the doping proportion of YOF:(Yb^{3+}, Er^{3+}) was 7 mass %, the short-circuit current density, the open-circuit voltage and the efficiency of the DSSC increased about 6.5, 6 and 23 % respectively. Wu et al. [99] and Dai et al. [93] reported similar structures using europium-ion-doped yttrium fluoride (YF_3:Eu^{3+}) and $Ca_3La_{3(1-x)}Eu_{3x}(BO_3)_5$ (CLBO:3xEu^{3+}) as a DC-luminescent material to convert UV to visible photons, respectively. These authors also observed effects of both light conversion and raising the Fermi level, attaining 32 % and 35 % increased efficiency of a DSSC sensitized with N719 dye relative to a DSSC with no luminescent material inside the photoanode layer [93,99].

The main challenge in applying a luminescent spectral converter in these configurations (Figure 9a and b) is a limited concentration of luminescent species applicable in the photoanode. On increasing the concentration of the luminescent spectral converter in the photoanode, the short-circuit current first increases and then decreases, but the increased concentration of rare-earth doping in TiO_2 led to an increased open-circuit voltage. In the effect of the concentration of luminescent species on the efficiency of power conversion of the cell, compromise hence exists between decreased J_{SC} and increased V_{OC}; the efficiency of the DSSC decreased on increasing the luminescent material above a critical concentration. This effect is attributed mainly to the crystal defects produced by the large proportion of luminescent species in the photoanode layer [76,82,86,91–96,98,99,101,106]. These defects can capture the photo-induced electrons and holes, leading to a

decreased photocurrent. The concentration of spectral-converter material also affects the surface area available for dye adsorption [78,101]. There is hence also a compromise between the concentration of luminescent material embedded inside the photoanode and the amount of dye loading. Although an increased concentration of luminescent material led to the conversion of an increased number of (to be wasted) photons, the short-circuit current decreased through the considerable loss of dye molecules. At a smaller concentration, the effect of spectral conversion compensated the current decrease caused by the decreased dye loading; when the concentration of spectral-conversion material was increased, the less available surface area and thereby smaller concentration of dye molecules led to a decreased photocurrent. This condition is more destructive when the photoanode is made of a single composite or doped TiO_2 layer (Figure 9a). In a double-layer structure (Figure 9b), the layer (thickness ~12 μm) of pure TiO_2 provides a large surface area to absorb the dye molecules; the dye loading is affected little by the concentration of luminescent particles [91,93–99]. Although dye molecules absorb on the surface of the luminescent species, these dye molecules cannot inject their electrons into the TiO_2 network and participate in the current generation. There is thus an optimum concentration of the luminescent material inside the photoanode, which can balance the effect of all these correlated factors and generate the greatest photocurrent. This optimum concentration varies in reports depending on the size of the particles, the QE and other matching parameters mentioned in section 2.

Using luminescent particles of nanometre size can help to increase the concentration of these particles in the photoanode without losing too much surface area available for dye loading [91,102]. Another solution to this problem is to cover the luminescent particles with a shell of TiO_2, which connects to the network of TiO_2 nanoparticles during the photoanode sintering and helps to collect the photo-generated electrons in the photoanode more effectively [77,87,106]. Zhang et al. used $NaYF_4$:Yb^{3+},Er^{3+}/TiO_2 core-shell nanoparticles to fabricate the photoanode of the DSSC; with this specific core-shell structure, the $NaYF_4$:Yb^{3+},Er^{3+} core absorbed and utilized infrared light, and the TiO_2 shell net concurrently effectively transmitted the electrons in the photoanode; both improved the conversion efficiency of the DSSC. DSSC with a $NaYF_4$: Yb^{3+},Er^{3+}/TiO_2 core-shell structure show efficiencies greater than that of a mixed photoanode. In the core-shell structural design, the TiO_2 shell forms a net structure resulting in an increased capability of electron transfer, which is an important factor to enhance the DSSC efficiency. For the mixed $NaYF_4$:Yb^{3+},Er^{3+} and TiO_2 photoanode, however, the luminescent nanoparticles and TiO_2 nanoparticles simply accumulate; the connection between the semiconductor TiO_2 nanoparticles is impeded by non-conducting luminescent nanoparticles, which block the electron transfer [77].

The TiO_2 shell provides also an effective surface area for dye loading on the luminescent particles because these dye molecules can inject their electrons into the TiO_2 shell and participate in the current generation. A TiO_2 shell thus can both enhance the dye loading ability and facilitate electron diffusion [106]. Meng et al. used UC composite Y_2O_3:Er/Au@TiO_2 (SYE/A@T) inside the scattering layer containing TiO_2 particles (size 200 nm) in a DSSC sensitized with N719 dye molecules [67]. In the core-shell structure, an Au nanoparticle-assisted plasmon effect can intensify the UC emission of Y_2O_3:Er; the TiO_2 coating can simultaneously both improve the charge transport within SYE/A@T and enlarge the dye-loading amount. The multifunctional scattering layer hence shows a light-absorbing range extended to the near-infrared region and improved light-scattering ability, leading to a significant improvement 27.6 % in efficiency of power conversion relative to a cell without SYE/A@T particles [67].

To overcome the problem of electron trapping, several researchers investigated an application of a non-conducting shell on the luminescent particles [76,83,101,106]. The luminescent particles introduced into the photoanode layer sometimes act as recombination centers and negate any increment attained via a spectral-conversion effect [76,97]. On covering the luminescent particles with an insulating shell, the luminescent cores are isolated from the external environment; the recombination effect, caused by surface defects and ligands, can be completely eliminated [101,106]. Chander et al. applied a shell of $NaYF_4$ on $NaYF_4$:Yb^{3+},Er^{3+} nanoparticles before introducing the UC luminescent particles into the TiO_2 layer [76]. The $NaYF_4$:Yb^{3+},Er^{3+}/$NaYF_4$ core-shell structure effectively prevented the capture of electrons because of the surface states and improved photo-emission. The DSSC fabricated with UC nanoparticles (average size 25 nm) showed enhanced overall power conversion efficiency ~12.5 % (sensitized with black/N749 dye) and of ~5.5 % (sensitized with N719 dye) under AM1.5G illumination [76]. This variation in the enhancement of the efficiencies for DSSC sensitized with varied dye molecules is attributed to the variation in the ASM, ESM and PA parameters induced by a difference in the absorption bands of the various dyes. Liang et al. prepared a highly uniform core-double-shell structure β-$NaYF_4$:Yb^{3+},Er^{3+}@SiO_2@TiO_2 in which amorphous SiO_2 as inner shell provided electrical isolation for the UC core and the outer TiO_2 prevented a decreased dye loading [101,106]. A similar core-double-shell structure, β-$NaYF_4$:Yb^{3+}, Er^{3+}@SiO_2@Au, was utilized for a multifunctional layer on top of the transparent TiO_2 layer in N719-sensitized DSSC by Zhao et al. [103]. $NaYF_4$:Yb,Er@SiO_2 particles of size 200-300 nm play a role of effective light-scattering centers and UC centers, and improved the efficiency of power conversion of the cell by 5.5 %. After attachment of the Au nanoparticles (20 nm) on the surface of $NaYF_4$:Yb,Er@SiO_2 particles, the efficiency of power conversion was enhanced 14.8 % relative to a cell without the multifunctional layer. This further improvement was attributed to the localized surface-plasmon resonance and enhanced UC effect in this layer.

Shan et al. showed that the vicinity of the luminescent particles and FTO in the DSSC has a negative effect on current generation [97]; they attributed this phenomenon to the electronic conduction of the luminescent material itself, which affected negatively the charge separation in the DSSC. They compared the performance of DSSC with double-layer photoanodes in various orders: FTO-pure TiO_2 layer-composite layer and FTO-composite layer-pure TiO_2 layer. No enhanced photocurrent was observed for the devices in which the composite layer served as the first layer directly on the FTO-glass. Although the photo-induced charge generation was enhanced with a composite layer, charge recombination apparently resulted in a decreased overall efficiency when the composite layer was near the FTO-glass [97]. When the double-layer structure (Figure 9b) was used, the composite layer was hence not placed next to the FTO. The

application of core-shell particles with an insulator shell can eliminate this problem [76].

Although a utilization of small luminescent particles might be more favorable so as not to lose much surface area for dye loading, an incorporation of larger particles into the photoanode grants a new functionality to them. Sub-micrometre particles can trap the incident light inside the photoanode by scattering visible photons. The presence of luminescent particles (sub-micrometre size) in the photoanode can improve the light-harvesting phenomenon through both spectral conversion and a scattering effect [87,88,101,102]. Roh et al. used single-crystalline, octahedral CeO_2:Eu^{3+} crystals inside a photoanode layer of DSSC sensitized with N719 in a double-layer structure [102]; the composite layer showed a great diffuse-reflection property (more than 70 %) in the visible part of the spectrum because of the size of CeO_2:Eu^{3+} particles (300−400 nm), as well as their mirror-like facets. The CeO_2:Eu^{3+}-based DSSC exhibited an efficiency of power conversion increased 14 % relative to a conventional TiO_2 nanoparticle-based DSSC, because of the strong light-scattering and DC effect of the CeO_2:Eu^{3+} crystals [102]. Liao et al. tried to generate a single-layer photoanode structure embedding $Na_xGdF_yO_z$:Yb/Er@TiO_2 hollow spheres into the TiO_2 layer [87]; they showed that an implementation of $Na_xGdF_yO_z$: Yb/Er@TiO_2 hollow spheres in the DSSC imparted light trapping through the light scattering from the submicrometre hollow spheres and the harvesting of near-infrared solar photons by the UC material, thereby resulting in an increased short-circuit current density, and an efficiency of power conversion increased 11.3 % [87]. As mentioned above, a TiO_2 shell effectively decreases the charge-transfer resistance in the photoanode containing luminescent $Na_xGdF_yO_z$: Yb/Er@TiO_2 hollow spheres.

A separate layer of luminescent particles has sometimes been used inside the DSSC on the TiO_2 mesoporous layer [52,106–109]. This configuration, shown in Figure 9c, is commonly applied for the purpose of utilizing the scattering property as well as spectral conversion. As the luminescent spectral-conversion layer was separate from the dye-loaded mesoporous semiconductor layer in this configuration, the complications originated from the size and concentration of luminescent particles; their surface properties were eliminated. There is hence no constraint on the size of the luminescent particles unless the luminescent QE is affected, but larger particles are preferred to provide a superior scattering property [52,106–108]. Particles of size several hundred nanometres [106,108] up to several micrometres [52,107] have served for this purpose. Improvements have been achieved with this configuration (Figure 9c) greater than for the configurations in which the luminescent particles are introduced inside the mesoporous TiO_2 layer (Figure 9a, b); this effect is attributed to an increased concentration of luminescent particles applied as spectral converter. The main consideration on applying a luminescent layer in configuration c is the porosity of the luminescent layer, which must be porous enough not to disturb the ion diffusion in the electrolyte. To make such a configuration, we prepared a phosphor paste using Terpineol, ethyl cellulose and ethanol according to the common method to make a TiO_2 paste for DSSC [52]. After fabrication of the TiO_2 layer on FTO-coated glass, the phosphor paste was coated on the TiO_2 layer. Treatment at 500 °C produced a thick porous layer of phosphor particles on the TiO_2 layer with effective adhesion. The luminescent layer acted as a dual functional layer and enhanced the short-circuit current density by 64 % via both a scattering effect and down-shifting the photons in spectral range 400–600 nm to photons in spectral range 600–800 nm. Although the luminescent layer was thick (160 μm), the porosity of this layer helped not to disturb the ion diffusion [52].

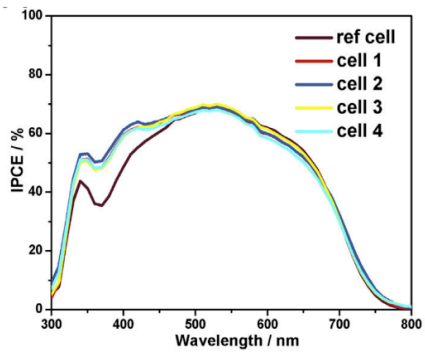

Figure 10. IPCE spectra of DSSC fabricated with varied electrolytes containing perylene. Cell 1, 2, 3, 4 represent perylene at 0.02, 0.05, 0.10 and 0.15 M added to the control electrolyte. Reproduced with permission from [110]

The next possible configuration to apply a material for spectral conversion inside the DSSC is shown in Figure 9d; in this configuration, the luminescent species are dispersed in the electrolyte. Being apart from the mesoporous TiO_2 layer, the dispersion of the luminescent particles inside the electrolyte does not affect the dye-loading amount or the electron transport through the photoanode layer, but can disturb the ion transport in the electrolyte if used in large concentrations [54,55,110]. Bai et al made a glowing electrolyte on adding fluorescent perylene to a conventional I^-/I_3^- electrolyte [110]. The transmitted UV photons from the photoanode layer converted by perylene to visible photons of wavelength 450-550 nm, which could be more efficiently utilized by the DSSC. The DSSC of perylene at optimal concentration 0.05 M in the electrolyte showed an efficiency of power conversion increased 11.6 % relative to a reference DSSC through an improved IPCE and thereby increased J_{SC}. Figure 10 shows the IPCE of devices with perylene at varied concentration in the electrolyte together with the IPCE of the control device; the increased IPCE in wavelength region 300-450 nm, matching the absorption band of perylene, clearly shows the effective down-shifting property of this luminescent material [110]. Bai et al. showed that redundant dispersed perylene in the electrolyte would make it more difficult for iodides to flow into the photo-electrode, thus increasing the transfer resistance between the TiO_2 conduction band and I_3^- in the electrolyte [110]. Kim et al. reported an application of rare-earth-doped phosphor particles in the electrolyte to improve the light-harvesting efficiency by light conversion [54,55]; for a DSSC sensitized with C106 dye, they achieved an efficiency of power conversion increased 3 % and 5 % on application of DC t-$LaVO_4$:Dy^{3+} and UC $NaYF_4$:Yb^{3+},Er^{3+} inside the iodide electrolyte, respectively [54,55]. They sought also to put a layer of luminescent particles inside or outside the DSSC; for the former luminescent materials, the efficiency of power conversion of a DSSC with a phosphor both positioned on the TiO_2 film and dispersed into the iodide electrolyte improved by 8 % [55], whereas using the UC

phosphor showed an efficiency of power conversion increased 21 % for a DSSC with phosphors contained in both the iodide electrolyte solution and an additional phosphor- reflecting film [54]. The other possible configuration for application of a spectral converter inside the DSSC is shown in Figure 9e. In this configuration, the LL is coated on the Pt-coated electrode; if having sufficient porosity not to stop I_3^- ions from reaching the Pt layer, this configuration might offer some advantages. The concentration of the spectral-converter particles can be tuned much more easily because it is unaffected by the concentration of dye loading or electron transport in the DSSC. It can also play a role as a scattering layer such that front illumination is applicable for such a configuration. No report of a fabrication of devices with such a configuration is available.

5. Summary and Outlook

In this review we have presented an overview of the potential that luminescent materials hold to adapt the absorption spectrum of a DSSC to an improved match with the solar spectrum, so to improve the efficiency of power conversion. Luminescent materials can effect spectral conversion through a DC, DS or UC process. The appropriate luminescent material for this purpose can be chosen from inorganic quantum dots or organic dyes or inorganic phosphors, and must satisfy specific requirements to maximize the benefits from an application of this strategy. These requirements are briefly discussed in section 2; in subsequent sections, we focus on the potential structural designs to employ a strategy for spectral conversion in DSSC.

These structural designs are classifiable in two groups: i) DSSC with the spectral converter outside the cell and ii) DSSC with the spectral converter inside the cell. In the former case, the DSSC can be designed so that the spectral-converter layer is transmissive or reflective; the choice of transmissive or reflective structure is based mainly on the transparency of the LL. In a transmissive configuration the LL must obviously be totally transparent with almost zero PA; an opaque LL is useless in this configuration. The reflective structure eliminates the need for a scattering layer inside the DSSC as the LL can have a dual functionality in reflective structures as both spectral converter and back-reflecting layer. The thickness of the LL and the concentration of the luminescent material used in this layer are also not limited in a reflective configuration. In a reflective structure a mirror-like layer might be placed at the back of the LL to reflect the emitted photons towards the DSSC whereas in a transmissive configuration, a portion of the emitted photons inevitably escapes from the air-LL interface. Much improvement is hence expected for a DSSC with a spectral converter in a reflective configuration compared with an analogous bare DSSC in a transmissive counterpart. In a previous publication [53], we estimated the highest attainable current density for DSSCs with spectral conversion layer outside the device in both transmissive and reflective configurations. Our results indicate that the device with a reflective configuration attained a maximal J_{sc} value (22.1 $mAcm^{-2}$) that is superior to that with a transmissive configuration (19.0 $mAcm^{-2}$), which is attributed to the presence of two important loss channels in the transmissive configuration, namely, reflection loss and escape cone loss. The maximum achievable current density calculated for the reflective configuration is in good agreement with the maximum current density for a DSSC with absorption onset at 800 nm calculated by Snaith [72] which confirms that the reflective configuration has potential for compensating the absorption losses in DSSC devices.

which confirms that the R-LDS idea has potential for compensating the absorption losses in DSSC devices.

The second category includes a more diverse design because of the high flexibility of the DSSC in incorporating luminescent particles inside the cell. The luminescent materials might be introduced into the photoanode or electrolyte, or placed on the photoanode or counter electrode as a separate layer. We discuss in detail each such configuration in section 4, considering the advantages and superiority of each along with difficulties and complications added to the fabrication. When the luminescent material is incorporated inside the photoanode layer either by making a composite paste or by doping TiO_2 particles, the size and concentration of the luminescent species are limited in the photoanode as a large concentration or large luminescent particles can cause recombination of charge carriers or diminished dye loading on decreasing the available surface area for dye adsorption. Incorporating rare-earth ions in the photoanode offers an improvement in the open-circuit voltage of the DSSC by *p*-type doping of the TiO_2 particles. The limitation on concentration is less critical when the spectral converter is introduced inside the DSSC as a separate LL on the photoanode or Pt counter electrode. In these cases, the LL generally provides a dual functionality as both scattering and spectral-converter layer. The application of larger luminescent particles with large refractive index is hence preferable for these configurations. The luminescent particles might disperse in the electrolyte to serve as a spectral converter. The limitation of the concentration of luminescent particles is also serious in this configuration as these particles can disturb the ion diffusion in the electrolyte.

The reports on direct comparison between the performance of spectral conversion strategy inside and outside the DSSC are limited to one by Kim et al. [54], who showed that a spectral-converter layer outside the DSSC in a reflective configuration (as Figure 5c) can improve the light-harvesting efficiency much more than when the spectral converter material is placed on the TiO_2 photoanode layer or dispersed in the electrolyte. This effect is expected as there is no limitation on the concentration of the spectral-converter material in the LL outside the DSSC; it can serve as both spectral-converter layer and scattering layer when placed in a reflective configuration. Although one cannot state definitely that a spectral converter outside the DSSC invariably shows a performance better than inside the DSSC, the former configuration definitely offers superiority as easier fabrication, no limitation on concentration or thickness of the LL in the reflective structure, and dual functionality as both scattering layer and spectral-conversion layer in the reflective structure, but the important point in this review is that, no matter where the spectral converter is present -- whether inside or outside the DSSC, a considerably improved J_{SC} is attainable with an appropriate choice of spectral converter and dye couple. The quantified parameters in this regard are introduced in section 2. For an ideal spectral converter-dye couple, ASM, ESM, PA, RO and QE have the values 1, 1, 0, 0 and 1 respectively.

The results collected here clearly confirm the potential of the spectral-conversion strategy to improve the light-harvesting efficiency in DSSC. Grätzel et al. reported a DSSC that achieves

large power-conversion efficiencies up to 28.9 % under conditions of room light [113]. This result encourages an idea that the DSSC holds particular promise as small modules to power portable electronic devices. The development of a spectral-conversion strategy might facilitate the commercialization of DSSC along that direction. However, much efforts are required for this strategy to find practical applications. Besides the choice of the proper architecture of the DSSC, the main challenge in order to gain a remarkable improvement in light harvesting and thereby the efficiency of the DSSC is the choice of luminescent material and dye couple. Therefore, developing phosphors with wider absorption range and near unity luminescence quantum efficiency are required. Moreover, proper DSSC dye molecules should be developed with absorption peak at longer wavelengths (e.g. 1000 nm). Although reflective configuration is shown to be more efficient, developing phosphor blends with high transparency would open new application areas including luminescent concentrator sheets, with the DSSCs located at the edges. This may highly decrease the cost of the energy conversion.

Keywords: Dye-sensitized solar cell • Light harvesting • Luminescence • Rare Earths • Spectral

[1] M. A. Green, K. Emery, Y. Hishikawa, W. Warta, E. D. Dunlop, *Prog. Photovoltaics Res. Appl.* **2016**, *24*, 905–913.
[2] M. A. Green, K. Emery, Y. Hishikawa, W. Warta, E. D. Dunlop, *Prog. Photovoltaics Res. Appl.* **2015**, *23*, 1–9.
[3] A. Hagfeldt, G. Boschloo, L. Sun, L. Kloo, H. Pettersson, *Chem. Rev.* **2010**, *110*, 6595–6663.
[4] J. Bisquert, *ChemPhysChem* **2011**, *12*, 1633–1636.
[5] J.-W. Shiu, C.-M. Lan, Y.-C. Chang, H.-P. Wu, W.-K. Huang, E. W.-G. Diau, *ACS Nano* **2012**, *6*, 10862–10873.
[6] L.-L. Li, E. W.-G. Diau, *Chem. Soc. Rev.* **2013**, *42*, 291–304.
[7] J.-H. Yum, E. Baranoff, S. Wenger, M. K. Nazeeruddin, M. Grätzel, *Energy Environ. Sci.* **2011**, *4*, 842–857.
[8] S. K. Balasingam, M. Lee, M. G. Kang, Y. Jun, *Chem. Commun.* **2013**, *49*, 1471–1487.
[9] C.-M. Lan, H.-P. Wu, T.-Y. Pan, C.-W. Chang, W.-S. Chao, C.-T. Chen, C.-L. Wang, C.-Y. Lin, E. W.-G. Diau, *Energy Environ. Sci.* **2012**, *5*, 6460–6464.
[10] H.-P. Wu, Z.-W. Ou, T.-Y. Pan, C.-M. Lan, W.-K. Huang, H.-W. Lee, N. M. Reddy, C.-T. Chen, W.-S. Chao, C.-Y. Yeh, et al., *Energy Environ. Sci.* **2012**, *5*, 9843–9848.
[11] A. Yella, H.-W. Lee, H. N. Tsao, C. Yi, A. K. Chandiran, M. K. Nazeeruddin, E. W.-G. Diau, C.-Y. Yeh, S. M. Zakeeruddin, M. Grätzel, *Science* **2011**, *334*, 629–634.
[12] K. Kakiage, Y. Aoyama, T. Yano, K. Oya, J. Fujisawa, M. Hanaya, *Chem. Commun.* **2015**, *51*, 15894–15897.
[13] S. P. Bremner, M. Y. Levy, C. B. Honsberg, *Prog. Photovolt Res. Appl.* **2008**, *16*, 225–233.
[14] B. E. Hardin, E. T. Hoke, P. B. Armstrong, J. Yum, P. Comte, T. Torres, J. M. J. Frechet, K. Nazeeruddin, M. Gratzel, M. D. McGehee, *Nat. Photonics* **2009**, *3*, 406–411.
[15] J.-H. Yum, B. E. Hardin, S.-J. Moon, E. Baranoff, F. Nüesch, M. D. McGehee, M. Grätzel, M. K. Nazeeruddin, *Angew. Chem., Int. Ed.* **2009**, *48*, 9277–9280.
[16] J. Yum, E. Baranoff, B. E. Hardin, E. T. Hoke, M. D. McGehee, F. Nüesch, M. Grätzel, M. K. Nazeeruddin, *Energy Environ. Sci.* **2010**, *3*, 434–437.
[17] Y.-J. Lin, J.-W. Chen, P.-T. Hsiao, Y.-L. Tung, C.-C. Chang, C.-M. Chen, *J. Mater. Chem. A* **2017**, *5*, 9081–9089.
[18] H. Lian, Z. Hou, M. Shang, D. Geng, Y. Zhang, J. Lin, *Energy* **2013**, *57*, 270–283.
[19] X. Liu, J. Qiu, *Chem. Soc. Rev.* **2015**, *44*, 8714–8746.
[20] D. Chen, Y. Wang, M. Hong, *Nano Energy* **2012**, *1*, 73–90.
[21] S. Liu, W. Chen, Z. Wang, *J. Nanosci. Nanotechnol.* **2010**, *10*, 1418–1429.
[22] J. de Wild, A. Meijerink, J. K. Rath, W. G. J. H. M. van Sark, R. E. I. Schropp, *Energy Environ. Sci.* **2011**, *4*, 4835–4848.
[23] P. Ramasamy, M. Palanisamy, J. Kim, *RSC Adv.* **2014**, *4*, 34873–34895.
[24] B. M. van der Ende, L. Aarts, A. Meijerink, *Phys. Chem. Chem. Phys.* **2009**, *11*, 11081–11095.
[25] N. Yao, J. Huang, K. Fu, X. Deng, M. Ding, X. Xu, *RSC Adv.* **2016**, *6*, 17546–17559.
[26] J. C. Goldschmidt, S. Fischer, *Adv. Opt. Mater.* **2015**, *3*, 510–535.
[27] M. G. Debije, P. P. C. Verbunt, *Adv. Energy Mater.* **2012**, *2*, 12–35.
[28] M. B. de la Mora, O. Amelines-Sarria, B. M. Monroy, C. D. Hernández-Pérez, J. E. Lugo, *Sol. Energy Mater. Sol. Cells* **2017**, *165*, 59–71.
[29] Z. Hosseini, W.-K. Huang, C.-M. Tsai, T.-M. Chen, N. Taghavinia, E. W.-G. Diau, *ACS Appl. Mater. Interfaces* **2013**, *5*, 5397–402.
[30] H. J. Hovel, R. T. Hodgson, J. M. Woodall, *Sol. Energy Mater.* **1979**, *2*, 19–29.
[31] C. K. Huang, Y. C. Chen, W. B. Hung, T. M. Chen, K. W. Sun, W.-L. Chang, *Prog. Photovoltaics Res. Appl.* **2013**, *21*, 1507–1513.
[32] R. Rothemund, S. Kreuzer, T. Umundum, G. Meinhardt, T. Fromherz, W. Jantsch, *Energy Procedia* **2011**, *10*, 83–87.
[33] Z. Cheng, F. Su, L. Pan, M. Cao, Z. Sun, *J. Alloys Compd.* **2010**, *494*, 7–10.
[34] E. Klampaftis, D. Ross, K. R. McIntosh, B. S. Richards, *Sol. Energy Mater. Sol. Cells* **2009**, *93*, 1182–1194.
[35] J. Liu, K. Wang, W. Zheng, W. Huang, C. Li, X. You, *Prog. Photovoltaics Res. Appl.* **2012**, *21*, 668–675.
[36] F. Bettiol, B. S. Richards, K. R. McIntosh, G. Lau, J. N. Cotsell, K. Hanton, *Prog. Photovolt Res. Appl.* **2009**, *17*, 191–197.
[37] T. Trupke, M. A. Green, P. Würfel, *J. Appl. Phys.* **2002**, *92*, 1668–1674.
[38] B. Hong, *Sol. Energy Mater. Sol. Cells* **2003**, *80*, 417–432.
[39] D. Alonso-Álvarez, D. Ross, E. Klampaftis, K. R. McIntosh, S. Jia, P. Storiz, T. Stolz, B. S. Richards, *Prog. Photovoltaics Res. Appl.* **2015**, *23* 479–497.
[40] D. Ross, E. Klampaftis, J. Fritsche, M. Bauer, B. S. Richards, *Sol. Energy Mater. Sol. Cells* **2012**, *103*, 11–16.
[41] D. Alonso-álvarez, D. Ross, B. S. Richards, *proceeding Photovolt. Spec. Conf.* **2012**, 9–14.
[42] B. S. Richards, K. R. McIntosh, *Prog. Photovoltaics Res. Appl.* **2007**, *15*, 27–34.
[43] E. Klampaftis, D. Ross, S. Seyrling, A. N. Tiwari, B. S. Richards, *Sol. Energy Mater. Sol. Cells* **2012**, *101*, 62–67.
[44] A. Solodovnyk, PhD thesis, Friedrich-Alexander Universität Erlangen-Nürnberg (FAU), **2016**.
[45] T. F. Schulze, T. W. Schmidt, *Energy Environ. Sci.* **2015**, *8*, 103–125.
[46] E. Klampaftis, D. Ross, K. R. McIntosh, B. S. Richards, *Sol. Energy Mater. Sol. Cells* **2009**, *93*, 1182–1194.
[47] C. Stanley, A. Mojiri, G. Rosengarten, *Nanophotonics* **2016**, *5*, DOI 10.1515/nanoph-2016-0035.
[48] J. Liu, Q. Yao, Y. Li, *Appl. Phys. Lett.* **2006**, *88*, 173119–173122.
[49] F. Bella, G. Griffini, J.-P. Correa-Baena, G. Saracco, M. Gratzel, A. Hagfeldt, S. Turri, C. Gerbaldi, *Science* **2016**, *354*, 203–206.
[50] X. Hou, T. Xuan, H. Sun, X. Chen, H. Li, L. Pan, *Sol. Energy Mater. Sol. Cells* **2016**, *149*, 121–127.
[51] N. Chander, A. F. Khan, P. S. Chandrasekhar, E. Thouti, S. K. Swami, V. Dutta, V. K. Komarala, *Appl. Phys. Lett.* **2014**, *105*, 33904.
[52] Z. Hosseini, N. Taghavinia, E. W.-G. Diau, *Mater. Lett.* **2017**, *188*, 92–94.
[53] Z. Hosseini, E. W. G. Diau, K. Mehrany, N. Taghavinia, *ChemPhysChem* **2014**, *15*, 3791–3799.
[54] C. W. Kim, W. J. Shin, M. J. Choi, J. H. Lee, S. H. Nam, Y. D. Suh, Y. S. Kang, Y. S. Kang, *J. Mater. Chem. A* **2016**, *4*, 11908–11915.
[55] C. W. Kim, D. K. Kim, W. J. Shin, M. J. Choi, Y. S. Kang, Y. S. Kang, *Nano Energy* **2015**, *13*, 573–581.
[56] B. McKenna, R. C. Evans, *Adv. Mater.* **2017**, *29*, 1606491.
[57] Y. Jestin, in *Compr. Renew. Energy* (Ed.: A. Sayigh), Elsevier, **2012**, pp. 563–585.
[58] X. Huang, S. Han, W. Huang, X. Liu, *Chem. Soc. Rev.* **2013**, *42*, 173–

201.
[59] N. Chander, A. F. Khan, V. K. Komarala, *RSC Adv.* **2015**, *5*, 66057–66066.
[60] T.-H. Wang, T.-W. Huang, Y.-C. Tsai, Y.-W. Chang, C.-S. Liao, *Chem. Commun.* **2015**, *51*, 7253–7256.
[61] F. Bella, G. Griffini, M. Gerosa, S. Turri, R. Bongiovanni, *J. Power Sources* **2015**, *283*, 195–203.
[62] G. Griffini, F. Bella, F. Nisic, C. Dragonetti, D. Roberto, M. Levi, R. Bongiovanni, S. Turri, *Adv. Energy Mater.* **2015**, *5*, 1401312.
[63] M. Zahedifar, Z. Chamanzadeh, M. Madani, M. Moradi, N. Sharifpour, *J. Mater. Sci. Mater. Electron.* **2016**, *27*, 4447–4456.
[64] H. Ahmed, J. Doran, S. J. McCormack, *Sol. Energy* **2016**, *126*, 146–155.
[65] H.-J. Hwang, S.-J. Joo, S. A. Patil, H.-S. Kim, X.-J. Xue, Y. Zhou, W. W. Duley, Q. Qiao, X. Li, J. Fan, *Nanoscale* **2017**, *5*, 71–81.
[66] P. Ramasamy, J. Kim, *Chem. Commun.* **2014**, *50*, 879–81.
[67] F. Meng, Y. Luo, Y. Zhou, J. Zhang, Y. Zheng, G. Cao, X. Tao, *J. Power Sources* **2016**, *316*, 207–214.
[68] H. Ahmed, S. J. Mccormack, J. Doran, *Int. J. Spectrosc.* **2016**, *1*, 1–7.
[69] D. M. Han, H.-J. Song, C.-H. Han, Y. S. Kim, *RSC Adv.* **2015**, *5*, 32588–32593.
[70] G.-B. Shan, H. Assaaoudi, G. P. Demopoulos, *ACS Appl. Mater. Interfaces* **2011**, *3*, 3239–3243.
[71] M. Liu, Y. Lu, Z. B. Xie, G. M. Chow, *Sol. Energy Mater. Sol. Cells* **2011**, *95*, 800–803.
[72] B. H. J. Snaith, *Adv. Funct. Mater.* **2010**, *20*, 13–19.
[73] C. Miao, T. Liu, Y. S. Zhu, Q. L. Dai, W. Xu, L. Xu, S. Xu, Y. Zhao, H. W. Song, *Opt. Lett.* **2013**, *38*, 3340–3343.
[74] J. Shen, Z. Li, R. Cheng, Q. Luo, Y. Luo, Y. Chen, X. Chen, Z. Sun, S. Huang, *ACS Appl. Mater. Interfaces* **2014**, *6*, 17454–17462.
[75] N. Yao, J. Huang, K. Fu, X. Deng, M. Ding, M. Shao, X. Xu, *Electrochim. Acta* **2015**, *154*, 273–277.
[76] N. Chander, A. F. Khan, V. K. Komarala, S. Chawla, V. Dutta, *Prog. Photovoltaics Res. Appl.* **2016**, *24*, 692–703.
[77] J. Zhang, H. Shen, W. Guo, S. Wang, C. Zhu, F. Xue, J. Hou, H. Su, Z. Yuan, *J. Power Sources* **2013**, *226*, 47–53.
[78] Y. Li, K. Pan, G. Wang, B. Jiang, C. Tian, W. Zhou, Y. Qu, S. Liu, L. Feng, H. Fu, *Dalt. Trans.* **2013**, *42*, 7971–7979.
[79] N. Yao, J. Huang, K. Fu, S. Liu, E. Dong, Y. Wang, X. Xu, M. Zhu, B. Cao, *J. Power Sources* **2014**, *267*, 405–410.
[80] Z. Zhang, Z. Cui, K. Zhang, Y. Feng, S. Meng, *J. Electrochem. Soc.* **2016**, *163*, A644–A649.
[81] H. Hafez, M. Saif, M. S. A. Abdel-Mottaleb, *J. Power Sources* **2011**, *196*, 5792–5796.
[82] R. Liu, L.-S. Qiang, W.-D. Yang, H.-Y. Liu, *J. Power Sources* **2013**, *223*, 254–258.
[83] Y. Li, W. Guo, H. Hao, L. Wang, Q. Su, S. Jin, L. Qin, W. Gao, G. Liu, Z. Hu, *Electrochim. Acta* **2015**, *173*, 656–664.
[84] M. J. Lim, Y. N. Ko, Y. Chan Kang, K. Y. Jung, *RSC Adv.* **2014**, *4*, 10039.
[85] Y. Li, G. F. Wang, K. Pan, B. J. Jiang, C. G. Tian, W. Zhou, H. G. Fu, *J. Mater. Chem.* **2012**, *22*, 20381–20386.
[86] L. Liang, Y. Yulin, Z. Mi, F. Ruiqing, Q. Lele, W. Xin, Z. Lingyun, Z. Xuesong, H. Jianglong, *J. Solid State Chem.* **2013**, *198*, 459–465.
[87] W. Liao, D. Zheng, J. Tian, Z. Lin, *J. Mater. Chem. A* **2015**, *3*, 23360–23367.
[88] G. Yuan, M. Li, M. Yu, C. Tian, G. Wang, H. Fu, *Sci. Rep.* **2016**, *6*, 37133.
[89] C. Zhang, Y. Xie, T. Bai, J. Hu, J. Wang, *J. Power Sources* **2015**, *297*, 16–22.
[90] H. Lai, Y. Wang, G. Du, W. Li, W. Han, *Ceram. Int.* **2014**, *40*, 6103–6108.
[91] J. Wang, J. Lin, J. Wu, M. Huang, Z. Lan, Y. Chen, S. Tang, L. Fan, Y. Huang, *Electrochim. Acta* **2012**, *70*, 131–135.
[92] S. Chen, J. Lin, J. Wu, *Appl. Surf. Sci.* **2014**, *293*, 202–206.
[93] W. B. Dai, Y. F. Lei, P. Li, L. F. Xu, *J. Mater. Chem. A* **2015**, *3*, 4875–4883.
[94] Q. Li, J. Lin, J. Wu, Z. Lan, Y. Wang, F. Peng, M. Huang, *Electrochim. Acta* **2011**, *56*, 4980–4984.
[95] J. Wu, J. Wang, J. Lin, Z. Lan, Q. Tang, M. Huang, Y. Huang, L. Fan, Q. Li, Z. Tang, *Adv. Energy Mater.* **2012**, *2*, 78–81.
[96] Q. Li, J. Lin, J. Wu, Z. Lan, J. Wang, Y. Wang, F. Peng, M. Huang, Y. Xiao, *Chinese Sci. Bull.* **2011**, *56*, 3114–3118.
[97] G. Bin Shan, G. P. Demopoulos, *Adv. Mater.* **2010**, *22*, 4373–4377.
[98] Q. Li, J. Lin, J. Wu, Z. Lan, Y. Wang, F. Peng, M. Huang, *J. Lumin.* **2013**, *134*, 59–62.
[99] J. Wu, J. Wang, J. Lin, Y. Xiao, G. Yue, M. Huang, Z. Lan, Y. Huang, L. Fan, S. Yin, et al., *Sci. Rep.* **2013**, *3*, 2058.
[100] J. Wu, G. Xie, J. Lin, Z. Lan, M. Huang, Y. Huang, *J. Power Sources* **2010**, *195*, 6937–6940.
[101] L. Liang, Y. Liu, C. Bu, K. Guo, W. Sun, N. Huang, T. Peng, B. Sebo, M. Pan, W. Liu, et al., *Adv. Mater.* **2013**, *25*, 2174–2180.
[102] J. Roh, S. H. Hwang, J. Jang, *ACS Appl. Mater. Interfaces* **2014**, *6*, 19825–19832.
[103] P. Zhao, Y. Zhu, X. Yang, X. Jiang, J. Shen, C. Li, *J. Mater. Chem. A* **2014**, *2*, 16523–16530.
[104] K.-W. Park, S. Ahn, S.-H. Lim, M. H. Jin, J. Song, S.-Y. Yun, H. M. Kim, G. J. Kim, K. M. Ok, J. Hong, *Appl. Surf. Sci.* **2016**, *364*, 573–578.
[105] H. Hafez, J. Wu, Z. Lan, Q. Li, G. Xie, J. Lin, M. Huang, Y. Huang, M. S. Abdel-Mottaleb, *Nanotechnology* **2010**, *21*, 415201.
[106] L. Liang, Y. Liu, X.-Z. Zhao, *Chem. Commun.* **2013**, *49*, 3958–3960.
[107] W. He, T. S. Atabaev, H. K. Kim, Y. H. Hwang, *J. Phys. Chem. C* **2013**, *117*, 17894–17900.
[108] G. Zhu, X. Wang, H. Li, L. Pan, H. Sun, X. Liu, T. Lv, Z. Sun, *Chem. Commun.* **2012**, *48*, 958–60.
[109] J. Bai, R. Zhao, G. Han, Z. Li, G. Diao, Z. G. Song, Y. Yang, D. C. Zhou, Z. Y. Yin, *RSC Adv.* **2015**, *5*, 43328–43333.
[110] S. Bai, L. Liang, C. Wang, H. F. Mehnane, C. Bu, S. You, Z. Yu, N. Cheng, H. Hu, W. Liu, et al., *J. Power Sources* **2015**, *280*, 430–434.
[111] P. Du, J. H. Lim, S. H. Kim, J. S. Yu, *Opt. Mater. Express* **2016**, *6*, 1896–1904.
[112] B. P. Rand, J. Genoe, P. Heremans, J. Poortmans, *Prog. Photovolt Res. Appl.* **2007**, *15*, 659–676.
[113] M. Freitag, J. Teuscher, Y. Saygili, X. Zhang, F. Giordano, P. Liska, J. Hua, S. M. Zakeeruddin, J.-E. Moser, M. Grätzel, et al., *Nat. Photonics* **2017**, *11*, 372–378.

REVIEW

Architectural design of DSSC for spectral conversion mechanism: Spectral conversion is a high potential strategy to improve the light-harvesting efficiency in DSSC. This review aims to cover all possible architectural designs of DSSC including spectral converter. Each configuration is discussed in details and important parameters governing the spectral conversion mechanism are introduced.

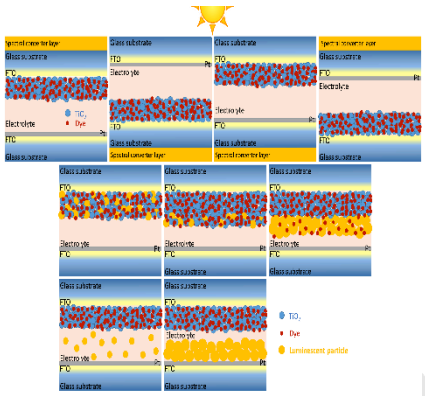

Zahra Hosseini, Nima Taghavinia, Eric Wei-Guang Diau*

Page No. – Page No.
Luminescent Spectral Conversion to Improve the Performance of Dye-sensitized Solar Cells